Journal of Colloid and Interface Science 388 (2012) 56–66

Contents lists available at SciVerse ScienceDirect

Journal of Colloid and Interface Science

www.elsevier.com/locate/jcis

In situ synthesis of gold nanoparticles in exponentially-growing layer-by-layer films

Liyan Shen [a,b], Laetitia Rapenne [a], Patrick Chaudouet [a], Jian Ji [b,*], Catherine Picart [a,*]

[a] LMGP, UMR 5628, Grenoble Institute of Technology and CNRS, Minatec, 3 parvis Louis Néel, F-38016 Grenoble Cedex, France
[b] MOE Key Laboratory of Macromolecular Synthesis and Functionalization, Department of Polymer Science and Engineering, Zhejiang University, Hangzhou 310027, China

ARTICLE INFO

Article history:
Received 25 April 2012
Accepted 29 June 2012
Available online 3 August 2012

Keywords:
Nanoparticles
Gold
Layer-by-layer
Biopolymers
Exponential growth
Polyamine
In situ reduction
High resolution transmission electron microscopy

ABSTRACT

In situ synthesis of inorganic nanoparticles (NPs) in polyelectrolytes multilayers (PEMs) has recently gained much attention. Due to the versatility of their composition, PEMs offer a unique opportunity to synthesize a variety of NPs. So far, mostly cationic precursors have been used and only few studies have investigated the possibility of using amine groups to bind anionic precursors. Here, we use exponentially growing poly(L-lysine)/hyaluronan (PLL/HA) films as a nanoreservoir to bind and sequester aurochlorate ($AuCl_4^-$) anions thanks to the large number of free amine groups. The polypeptide–polysaccharide reactive template enabled the formation in a spatially-confined environment of gold NP at a very high yield. The synthesized gold NPs were homogenous and well-dispersed in the nanocomposite. Importantly, there was no particular effect of the film-ending layer (either PLL or HA). The largest particles of ~9 nm and the largest amount of gold were obtained at acidic pH of 3. When the pH was increased, smaller and more numerous NPs were synthesized but the total amount of gold was lower. Based on UV–visible spectrometry, FTIR and TEM data, we finally propose a scheme for the mechanism of gold NPs formation, in which several groups of PLL and HA contribute to the binding of gold ions, the nucleation and growth of NPs, and their stabilization in the "bulk" of the film.

1. Introduction

Metal nanoparticles are used in an increasingly large number of biomedical applications [1] in the field of biotechnology, biosensing [2,3], bioimaging [4], and drug and gene delivery [5] due to their interesting optical and electrical properties. During the past years, several studies have focused on the directed assembly of metal nanoparticles into organic solutions to form organic–inorganic hybrid nanomaterials [6,7]. Hybrid nanocomposites are synthesized via two major strategies. The first consists in assembling prefabricated inorganic nanoparticles (NPs) with polymers, either by chemical grafting or by adsorption of the polymer onto the particles [8]. Assemblies of NPs and polyelectrolytes can be built in a layer-by-layer (LbL) fashion to control the number and position of nanoparticles [9–11], but the rinsing steps may possibly affect the stability of the assembly. The second uses an organic solution (or "matrix") as a template to nucleate and grow *in situ* inorganic NPs [12]. This is most often achieved directly by adding precursor ions into the polymeric solution [13]. However, the chemical synthesis of metal nanoparticles, including platinum, silver or gold, often requires the use of harsh chemicals (i.e. detergents, solvents), which are undesirable for biomedical applications [14]. In this respect, biomolecules such as peptides [15,16], proteins, or polysaccharides [17] are interesting due to the presence of numerous charged groups in their chains. This enables them to interact with positively charged or negatively charged metal ions precursors, thereby stabilizing them [18]. Typically, anionic groups can interact with Ag^+ [17] or Pb^{2+} ions [19] and cationic groups can interact with negatively charged ion complexes, such as gold aurochlorate ions ($AuCl_4^-$ or $AuCl_2^-$) [20]. Peptides can also contribute to the reduction of precursor ions by acting as electron donors [16]. Moreover, peptides can act as stabilizer of the formed nanoparticles, as they can specifically bind to certain inorganic surfaces [7].

Gold nanoparticles are particularly interesting due to their non-toxicity [14], biocompatibility, photothermal properties [21], ease of imaging and versatility of surface chemistry [22]. Polymers containing amine groups have been widely used as binding sites for gold aurochlorate ions ($AuCl_4^-$) and as stabilizer of gold nanoparticles [18,23–25]. Natural biopolymers such as α-amino-acids are also emerging as versatile templates [16], due to their capacity to reduce gold ions and to bind to Au^0. Importantly, not only do aromatic, amine or amide groups play a role in the synthesis of gold NPs, but other groups such as C—O—C and carboxylate have been shown to exhibit some reducing capacities [26,27].

Of particular interest are the possibility offered by biopolymers to control nanoparticle sizes and morphologies [28], and also to work in mild conditions, i.e. at ambient temperature, in non-toxic

* Corresponding authors. Fax: +86 571 879 53 729 (J. Ji), +33 (0)4 56 52 93 01 (C. Picart).
E-mail addresses: jijian@zju.edu.cn (J. Ji), catherine.picart@minatec.grenoble-inp.fr (C. Picart).

0021-9797/$ - see front matter © 2012 Elsevier Inc. All rights reserved.
http://dx.doi.org/10.1016/j.jcis.2012.06.079

solvents or even in aqueous medium. Typically, reduction of tetrachloroauric acid ($HAuCl_4$) can be achieved in a basic buffer such as sodium borate or by photo-chemical UV-irradiation [6], which generates the necessary electrons to catalyze the reaction. This opens new perspectives for the "green" biomimetic synthesis of nanocomposites. So far, the majority of studies have focused on formation of NPs from solutions containing a mixture of the biomacromolecule and of the metallic ions [18,20,26]. However, controlling the spatial organization, nucleation and growth of monodisperse and non-aggregated NPs on 2D material surfaces remains a challenge [29].

Polyelectrolyte multilayer films (PEMs) constitute a versatile and easy system to build architectures whose properties can be tuned in terms of thickness, film internal structure and degree of ionization of the polyelectrolytes [30,31]. Synthetic and/or biological polyelectrolytes that possess various functional groups, including carboxylic acid, amine, and amide, can be used as building blocks. The carboxylic groups of synthetic and natural polyanions have been used for the trapping of silver ions in PEM films and their subsequent reduction *in situ* [17,19,32,33]. The distribution of silver NPs within the film [19], their size [32,34] and the total silver loaded amount [33] can be tuned by controlling the film architecture.

It is only recently that the *in situ* synthesis of gold NPs in the bulk or at the surface of PEM films has been reported [12,29]. Tsukruk and coworkers showed that the deposition of the polyaminoacid poly(L-tyrosine) as topmost layer on a poly(allylamine)/poly(styrene sulfonate) (PAH/PSS) film, was able to direct nanoparticle formation [29]. In this case, gold NPs were confined to the topmost polyaminoacid layer due to absence of diffusion of gold ions in the underlying stitched films. The "bulk" of PEM films can potentially serve as nanoreservoir to synthesize NPs in a spatially confined environment [12]. Rubner and coworkers used the reducing properties of amine groups of PAH to synthesize gold NP within the bulk of polyacrylic acid/PAH (PAA/PAH) and (PAA/PSS) films. However, as these films grow linearly [35] and exhibit a high degree of ion pairing [36], they had to induce a nanoporosity transition by soaking them in a very acidic solution (pH < 2) to generate free ammonium group and to allow diffusion of gold chloride ions.

In this context, exponentially growing films [37,38] that are more swollen [39], are rich in unpaired amine groups and contain other functional groups (i.e. carboxylic acid, hydroxyl) may offer new potentialities for the loading of a high amount of gold ions as well as for their reduction. Poly(L-lysine)/hyaluronan (PLL/HA) films [37,38,40] that are now widely accepted as model exponentially growing PEM films appear as an interesting candidate. Here, we demonstrate that the *in situ* formation of gold NPs using UV-reduction can be controlled solely by varying the solution pH of the gold precursor solution. Homogenous gold NPs were formed at varying pH, with diameter ranging from ~1.7 nm (high pH) to ~9 nm (low pH). Very interestingly, the gold NPs were homogeneously dispersed throughout the entire film depth over ~2.5 μm at a very high yield. These results show for the first time that exponentially-growing PEM films rich in amine groups can be used as nanoreservoirs for the spatially-confined growth of a large amount of gold NPs.

2. Results and discussion

In this work, we used a biocompatible polypeptide/polysaccharide made by alternating deposition of PLL at pH 9.5 and HA at pH 2.9 (i.e. a (PLL9.5/HA2.9) film) as template for *in situ* synthesis of gold NPs in mild conditions, i.e. in pure water. The films were built as described in our previous studies by alternate deposition of the polyelectrolytes followed by a water rinse and blow drying after each deposited layer [40,41]. $(PLL9.5/HA2.9)_i$ films (i = 7.5 or 8, being the number of layer pairs) of typical thickness between 2 and 3 μm [40] have been used for all experiments. Aurochlorate ions were loaded as precursors by simple adsorption performed after film buildup. Here, we investigated the potentiality of these films to spatially confine the growth of gold NPs and to stabilize them. We focused on the effect of pH of the gold chloride solution, which is known to affect the stability of the Au–Cl–H_2O system [18], on nanoparticle formation. We also studied the influence of the film ending layer (PLL versus HA). We analyzed the effect of gold NP formation and film bulk structure by Fourier transform infrared spectroscopy (FTIR). Furthermore, we quantified the size of gold NPs and observed their distribution in the film cross-section by means of high resolution transmission electron microscopy (HR-TEM). Finally, the combination of UV–visible spectroscopy, FTIR and TEM data allowed us to propose a mechanism for NP formation within the PEM film.

2.1. In situ synthesis of gold nanoparticles in the bulk of (PLL/HA) multilayer films

We loaded the gold aurochlorate ions into $(PLL9.5/HA2.9)_7$-PLL9.5 films by soaking the film in 10 mM gold chloride solutions under acidic, neutral or basic conditions, which corresponded respectively to pH 3, 6 and 9. The films were then simply rinsed with water and air-dried before being analyzed by FTIR. Importantly, the film kept its integrity upon photo-reduction (Fig. S1) as indicated by the similarities between the FTIR spectra obtained prior to gold loading, after gold loading and after UV-irradiation. Qualitatively similar spectra were obtained for HA-ending films (data not shown). The *in situ* synthesis of gold NPs was followed via UV–visible spectrometry (Fig. 1) since it is well known that gold NPs exhibit a strong surface plasma resonance (SPR) band depending on the shape and size of nanoparticles [42,43]. Fig. 1 shows the spectra obtained over time for both PLL-ending (A–C) and HA-ending films (A′–C′) immersed in gold chloride solutions at different pH. For all pH conditions, an absorbance peak emerged in the range of 500–550 nm. It increased with the reduction time, which qualitatively indicated gold NPs were successfully synthesized [44]. The width of the peak of ~50 nm also indicated that the NPs were well-dispersed and rather spherical [45]. The reduction was completed in ~35 h. The maximum absorbance values for each condition were extracted and plotted as a function of the reduction time (Fig. 1D). The films loaded with gold chloride at pH 3 exhibited the largest increase in absorbance, followed by those loaded with the precursor solution at pH 6. When the pH of the precursor solution was of 9, a small but steady increase was observed. Of note, the ending layer of the films did not have a key role in the gold NPs formation process as both PLL-ending and HA-ending films behaved very similarly. These results qualitatively indicated that the amount of gold NPs formed was directly dependent on the pH of the precursor solution: the lower it was, the higher was the amount of NPs formed. Indeed, quantitative measurements of gold mass using inductively-coupled plasma mass spectrometry (ICP-MS) confirmed that the total mass of gold in the film was higher when gold aurochlorate was loaded at low pH (Table 1).

Furthermore, we plotted the maximal wavelength (λ_{max}) of the SPR peak as a function of the pH of the precursor solution (Fig. 1E). For PLL-ending as well as for HA-ending films, λ_{max} decreased when the pH increased, which qualitatively indicated that gold NPs were smaller at high pH [45]. These results qualitatively in agreement with previous results showing that the size of NPs formed in bulk solutions of poly(allylamine) was slightly modulated by the pH. It varied between 3.7 and 2.6 nm when the pH was increased from 1.5 to 12.5 [20], with a corresponding variation in λ_{max} of 6 nm [20]. Thus, the wavelength shift observed in our

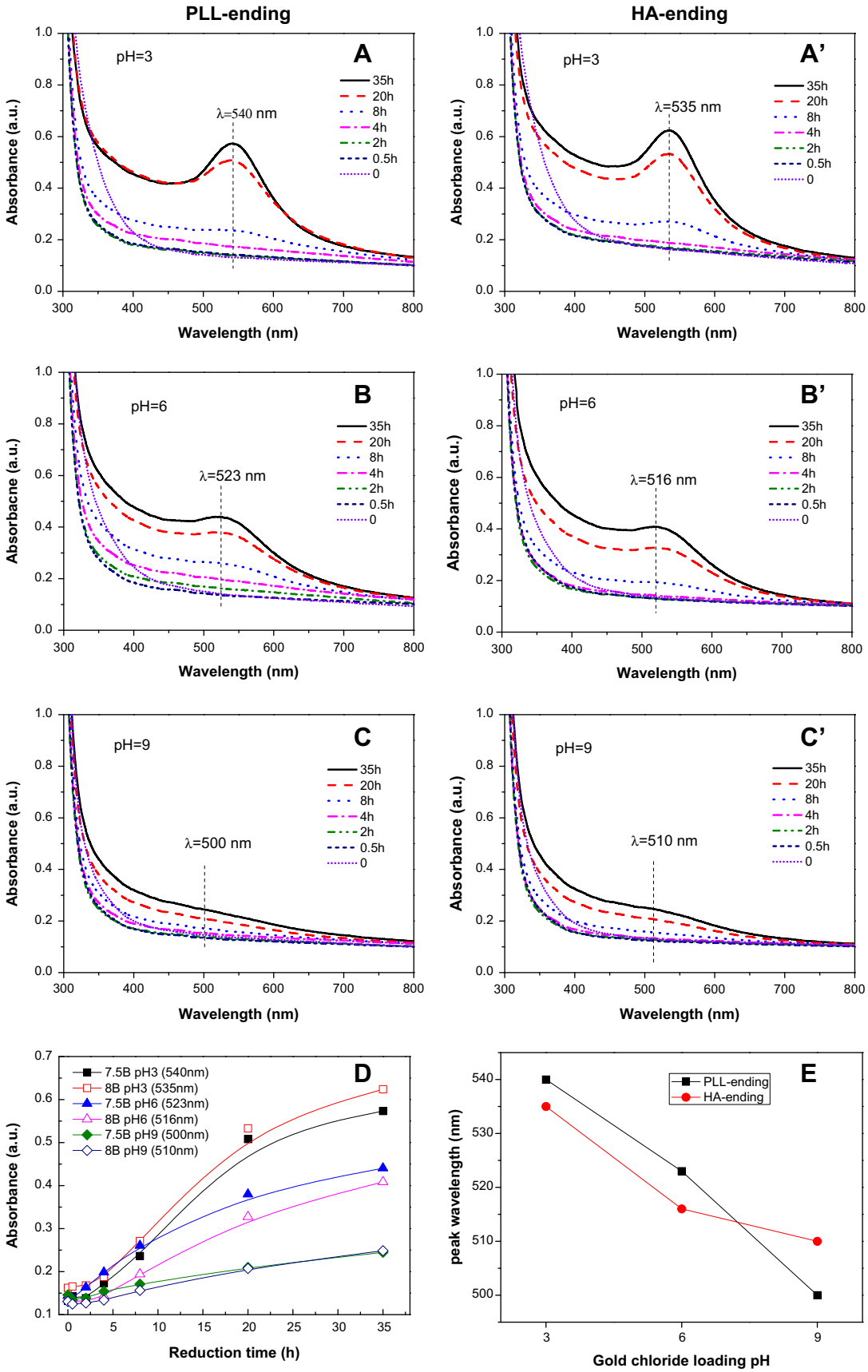

Fig. 1. UV–visible absorption spectra acquired at different time points during UV-photoreduction in $(PLL9.5/HA2.9)_7$-PLL9.5 films (A–C) and $(PLL9.5/HA2.9)_8$ films (A′–C′). Gold chloride was loaded at different pH: pH = 3 (A, A′), pH = 6 (B, B′) or pH = 9 (C, C′). (D) Maximum of the SPR peak plotted as a function of the reduction time. (E) Wavelength of the maximum SPR peak, plotted as a function of the pH of the precursor solution.

Table 1
Quantification by ICP-MS of the mass of gold synthesized *in situ* in the (PLL9.5/HA2.9) multilayer films and of the density of gold NP based on cross-sectional TEM images, in function of the pH of the gold chloride solution. PLL-ending and HA-ending films are respectively $(PLL9.5/HA2.9)_7$-PLL9.5 and $(PLL9.5/HA2.9)_8$ films.

Total gold mass (μg)	pH 3	pH 6	pH 9
PLL-ending films	12.8 ± 0.4	8.5 ± 0.4	6.6 ± 0.2
HA-ending films	11.9 ± 0.3	7.6 ± 4.6	7.1 ± 0.1
Gold NP density (particle/μm²)			
PLL-ending films	2500	26,000	63,000
Fold increase (compared to pH 3)	1	X 10.4	X 25.2

case (~40 nm for 6 pH units of difference from 3 to 9) indicated at first sight that the formed NPs were much bigger.

Further insight into the bulk organization of the nanocomposite films was obtained by scanning electron microscopy (SEM) (Fig. 2). Drastic differences between the different samples emerged. When the precursors were loaded at pH 3, gold NPs homogeneously covered the entire film surface and appeared as bright spots of various sizes (Fig. 2A and A′). Furthermore, the gold NPs were distributed throughout the whole film thickness over ~2.5 μm (Fig. 2A″). Of note, large gold crystals were also formed in the film/silicon interface. This may originate from the fact that the SiO_2 layer at the surface of the silicon substrate is positively charged at very low pH [46]. It may thus serve as nucleation site for gold chloride ions. As the loading pH increased to 6 (Fig. 2B and B′), homogeneously distributed gold NPs were observed at the film surface, but of smaller size than those observed at pH 3. However, no NPs could be visualized in the film cross-section at this magnification (Fig. 2B″). We noted that the film prepared at pH 9 (Fig. 2C–C″) was very difficult to observe due to charge effects. Here again, no NP was visualized in the cross-section at this magnification.

Meanwhile, we noticed that the film thickness increased after immersion in the Au-precursor solution of lower pH (Fig. 2A″–C″). This may due to a swelling of the film immersed in more acidic pHs of 6 and 3 [47]. Indeed, when the PLL-ending film (initially at pH 9.5), was immersed in Au-precursor solution of lower pH, COO^- gradually turned to be COOH and NH_2 gradually became NH_3^+. Thus, more positive charges and less negative charge are present when solution pH is lowered from 9 to 6 and then to 3. This may lead to swelling of the film and increase in film thickness.

Also, the surface and cross-section morphology of HA-ending films made of 8 layer pairs (Fig. SI2) were almost identical to their PLL-ending counterparts, except that the film thickness was about 0.5 μm thicker. Considering the very similar behavior of PLL-ending and HA-ending films regarding gold NP synthesis (Fig. 1), we next only focused on PLL-ending films.

Cross-sections of the films were observed by TEM at low (Fig. 3) and high resolution (HR-TEM) (Fig. 4). First, we noticed that gold NPs were always well dispersed throughout the whole film thickness, regardless of the pH of the gold chloride solution, which indicated that aurochlorate ions had diffused homogeneously in the film (Fig. 3). Here again, we observed that large NPs of 30–60 nm in diameter have nucleated at the silicon/film interface, in the case of pH 3. From these TEM images, we quantified the gold NP size distribution (Fig. 3A″–C″). The median size of gold NPs synthesized from pH 3, 6 and 9 was of 8.6, 2.8 and 1.7 nm, respectively. Thus, increasing the loading pH of gold chloride resulted in a significant decrease of the size of gold NPs. High resolution TEM imaging of the gold NPs was performed to investigate their nanocrystalline structure (Fig. 4). Parallel lattices of the nanocrystals were clearly observed for gold NPs synthesized in acid and neutral conditions (Fig. 4A′ and B′). Furthermore, the electron diffraction pattern confirmed the typical rings characteristic of a polycrystalline phase, which was indexed in the reciprocal space by superposition of

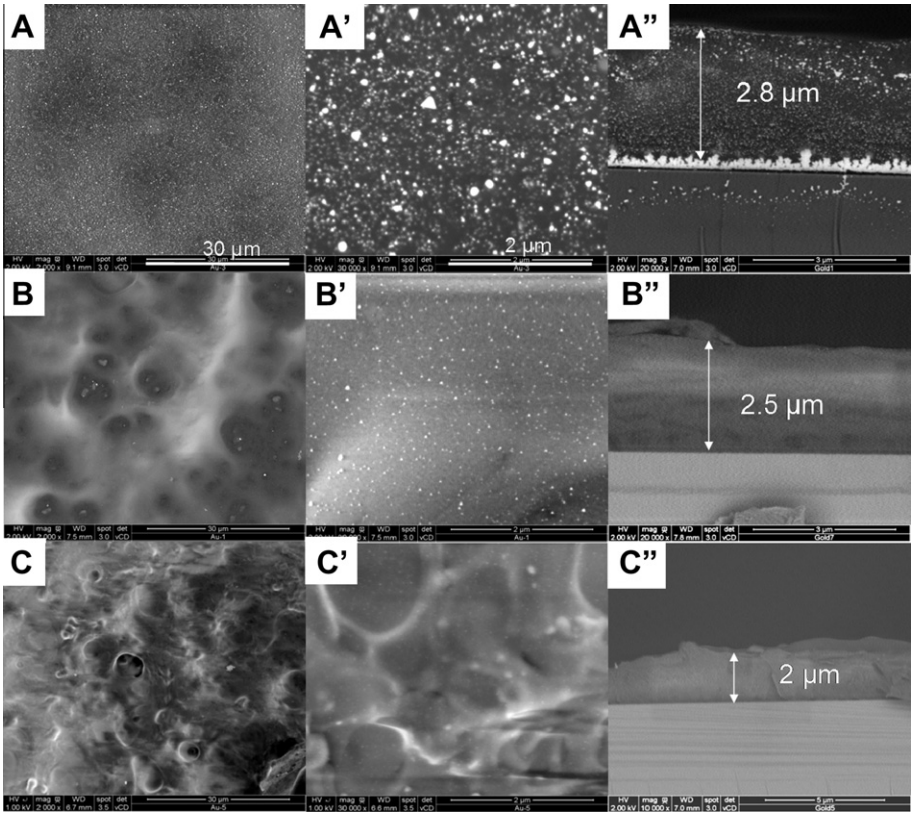

Fig. 2. SEM images of gold nanoparticles synthesized *in situ* in $(PLL9.5/HA2.9)_7$-PLL9.5 films: surface morphology at different magnifications (left and middle columns) and cross-sections (right column). Gold chloride was loaded at pH 3 (A–A″), 6 (B–B″), and 9 (C–C″). The scale bars are 30 μm for (A–C) and 2 μm for (A′–C′).

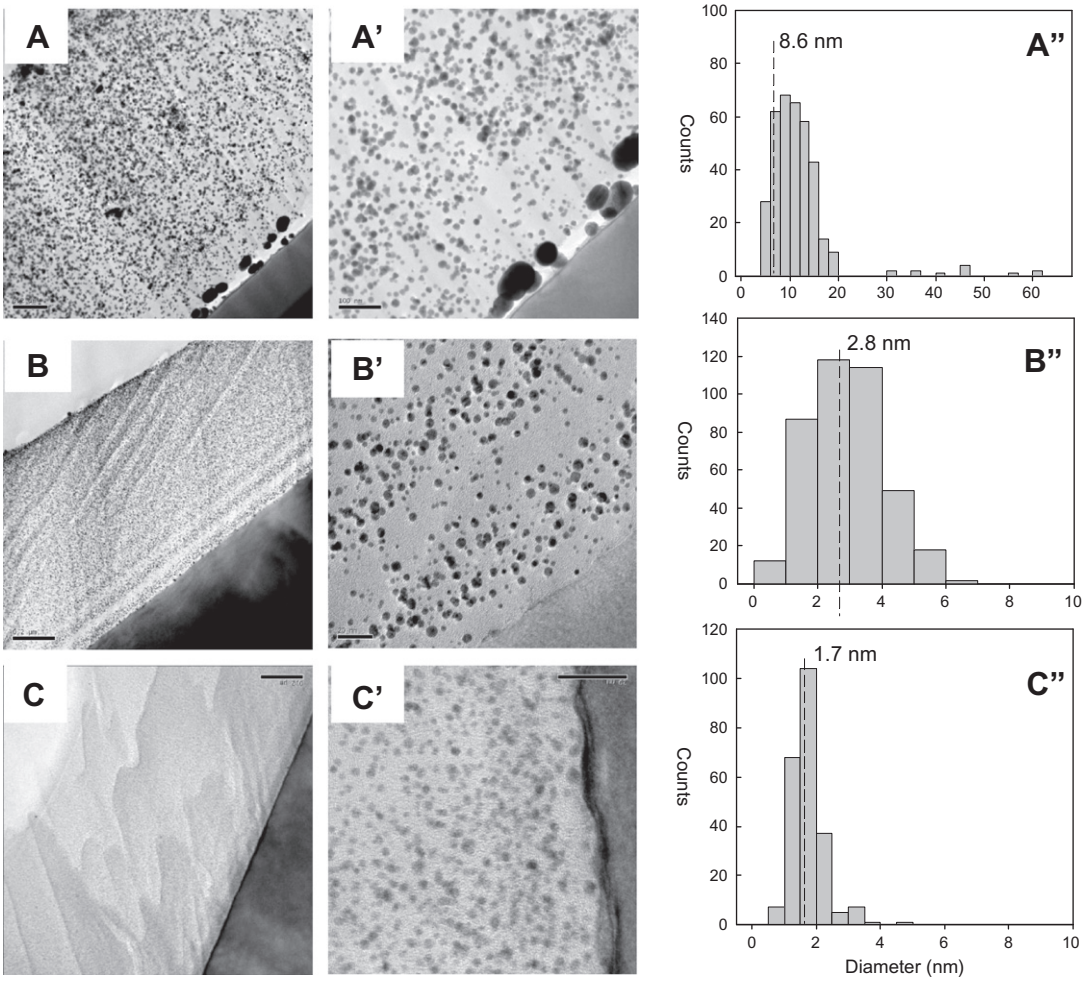

Fig. 3. Cross-sectional TEM images through $(PLL9.5/HA2.9)_7$-PLL9.5 films showing gold NPs dispersed over the entire film thickness. Gold chloride was loaded at different pH of 3 (A–A″), 6 (B–B″), and 9 (C–C″). Images are shown at different magnifications. The black zone corresponds to the silicon substrate and the white zone to Epoxy resin. The gold NPs were formed homogeneously throughout the whole film thickness, as observed by the presence of very small to large black dots. The corresponding particle size distribution deduced from these TEM images is given in figure A″, B″, C″. The dashed lines indicate the median NP size, which is of 8.6 nm, 2.8 nm and 1.7 nm, respectively for films loaded with gold chloride at pH 3, 6 and 9. Scale bars are 200 nm for (A–C) 100 nm for A′ and 20 nm for B′, C′.

the X-ray diffraction of Au powder (Fig. 4A″ and B″). Conversely, the gold NPs formed at pH 9 (Fig. 4C and C′) were too small to get enough electron diffraction signals (Fig. 4C″). However, the energy dispersive X-ray (EDAX) data confirmed the existence of gold NPs in these films as well (Fig. SI3). Based on TEM images of the cross-sections, the gold NP density was quantified for the different conditions. A 25-fold increase in NP density was observed when the pH was increased from 3 to 9 (Table 1).

Thus, (PLL9.5/HA2.9) films played the role of a nanoreservoir for gold aurochlorate ions and enabled the spatially-confined growth and stabilization of a very large number of gold NPs. The gold NPs were homogeneously dispersed in the bulk of the nanocomposite.

2.2. Possible mechanism of gold NPs photosynthesis in (PLL/HA) films

In order to understand the molecular mechanism underlying *in situ* synthesis of gold NPs in (PLL9.5/HA2.9) multilayer films and to investigate which functional groups were important, we performed additional experiments in solution using the gold chloride solution at different pH and the individual film components. Fig. 5 shows UV–visible spectra of a pure 1 mM $HAuCl_4$ solution adjusted to different pH and of this solution in the presence of either HA (3 mg/mL) or PLL (1 mg/mL), taken before and after UV irradiation (Fig. 5). The corresponding images of the solutions are shown in Fig. SI4. As shown in Fig. 5A, the absorbance of the $HAuCl_4$ solution at pH 3 exhibited a peak at ~313 nm, which can be attributed to the charge-transfer band from chloride *p* to gold *d* orbitals [48]. The corresponding images showed a slightly yellow color for this solution. This band disappeared when the pH of the solution was increased. The Au–Cl–H_2O system has been studied [18] and it is known that $AuCl_4^-$ is stable over a wide pH range (0–7.5) [49]. However, destabilization of the system at higher pH can lead to a transition to $AuCl_2^-$. Indeed, the Au^+ ions of $AuCl_2^-$ can be more easily reduced in Au^0 than Au^{3+} of $AuCl_4^-$ [50]. Increasing the pH to 6 and 9 probably resulted in destabilization of $AuCl_4^-$ with a subsequent transition to $AuCl_2^-$, which does not exhibit any specific peak in the UV–visible range. When HA was added to the $HAuCl_4$ solution, the UV–visible spectra were very similar to the case where no HA was present (Fig. 5B). In the case where PLL was mixed to the $HAuCl_4$ in solution, the charge-transfer band was shifted to ~385 nm (Fig. 5C) and the complex gave rise to a yellow color (Fig. SI4) [48]. The band was also broader and of lower intensity. This is compatible with the formation of ion complex between amine groups on PLL chains and gold ions:

$$COO^- - NH_3^+ + H^+ + Au^{3+}Cl_4^- \rightarrow COOH + NH_3^+Au^{3+}Cl_4^- \quad (1)$$

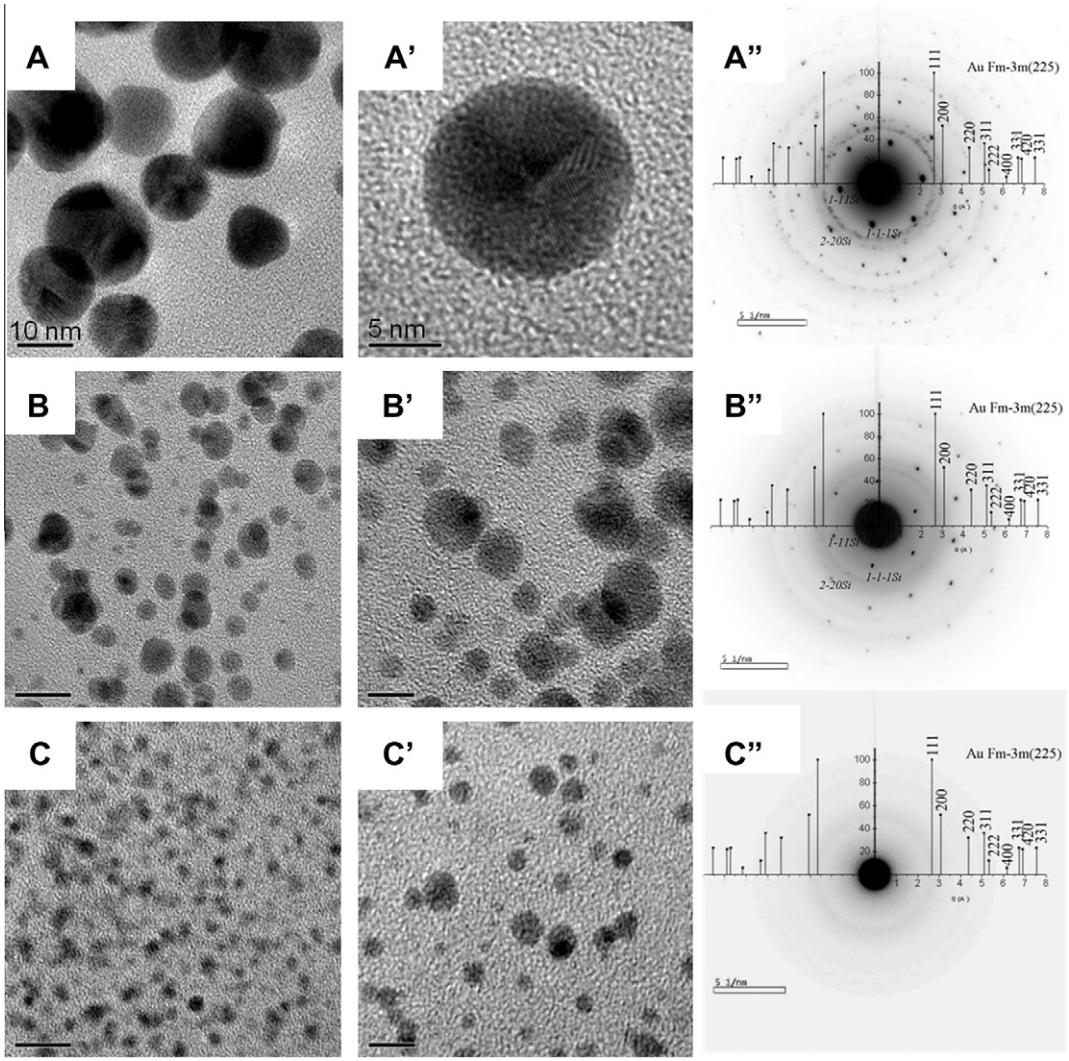

Fig. 4. High resolution TEM images of gold NPs synthesized *in situ* in $(PLL9.5/HA2.9)_7$-PLL9.5 films. (A, A′, B, B′, C, C′): the conditions for the pH are the same as for Fig. 3. The corresponding electron diffraction patterns of the samples are also shown (A″–C″). Scale bars are 10 nm for (A–C) and 5 nm for (A′–C′).

Thus, PLL can first play a role in the stabilization of the $AuCl_4^-$ ions and subsequently in the stabilization of the gold nuclei.

Research has shown that $AuCl_4^-$ can be excited by absorbing a photon and can be reduced to Au^{2+}, which is unstable and rapidly disproportionated to Au^{3+} and Au^+. Au^+ can be re-excited by absorbing another photon and finally be reduced to Au^0 [51]:

$$HAu^{3+}Cl_4^- \xrightarrow{h\nu} (HAu^{3+}Cl_4^-)^* \text{ excitation} \quad (2)$$

$$(HAu^{3+}Cl_4^-)^* \rightarrow HAu^{2+}Cl_3^- + Cl \text{ reduction} \quad (3)$$

$$2HAu^{2+}Cl_3^- \rightarrow HAu^{+}Cl_2^- + HAu^{3+}Cl_4 \text{ disproportionation} \quad (4)$$

$$HAu^{+}Cl_2^- \xrightarrow{h\nu} (HAu^{+}Cl_2^-)^* \text{ excitation} \quad (5)$$

$$(HAu^{+}Cl_2^-)^* \rightarrow Au^0 + HCl + Cl^- \text{ reduction} \quad (6)$$

$$nAu^0 \rightarrow (Au^0)_n \text{ rapid formation} \quad (7)$$

It has been proven that —CH_2—OH groups can serve as reducing agents to reduce gold ions that are in an excitation state [52,53]. These groups may be involved in steps (3) to (6) of the reactions to favor gold NP synthesis [44,51]. Of note, the UV reduction of gold precursors released H^+ and made the film more acid.

In our case, a weak and broad peak at ~550 nm was observed in the $HAuCl_4$ solution only at pH 9 (Fig. 5A′) after UV irradiation. The solution became blue with large and aggregated clusters (Fig. 5A′ inset). When HA was added to the $HAuCl_4$ solution, the change in the absorbance spectra was even larger, especially at pH 9 (Fig. 5B′ with a broader peak that was shifted to the right (~595 nm). A larger number of precipitated gold clusters were observed in this case (inset of Fig. 5B′).

In the case of PLL addition, a very small increase in UV absorbance at ~560 nm was noted after UV-reduction, especially at pH 9. The mixture at pH 9 exhibited a red color and contained well-dispersed NP of ~10 nm in size, as was observed by TEM (Fig. SI5). Thus, PLL appeared to act as good stabilizer of Au^0 atoms, as was previously observed for poly(ethylene imine) [18].

To further elucidate the chemical modifications inside the films, we investigated the changes in the FTIR spectra obtained at different steps of the procedure, highlighting the appearance or disappearance of specific groups. Fig. 6 shows different spectra obtained after loading with the gold chloride solution at different pHs (Fig. 6A–C) and after UV-irradiation (Fig. 6A′–C′). In parallel, control experiments were performed in which the films were only soaked in water at different pH, without any gold precursors, before being UV-irradiated.

Upon addition of the chloroaurate solution on a PLL-ending film, we observed specific differences in the FTIR spectra. First, we

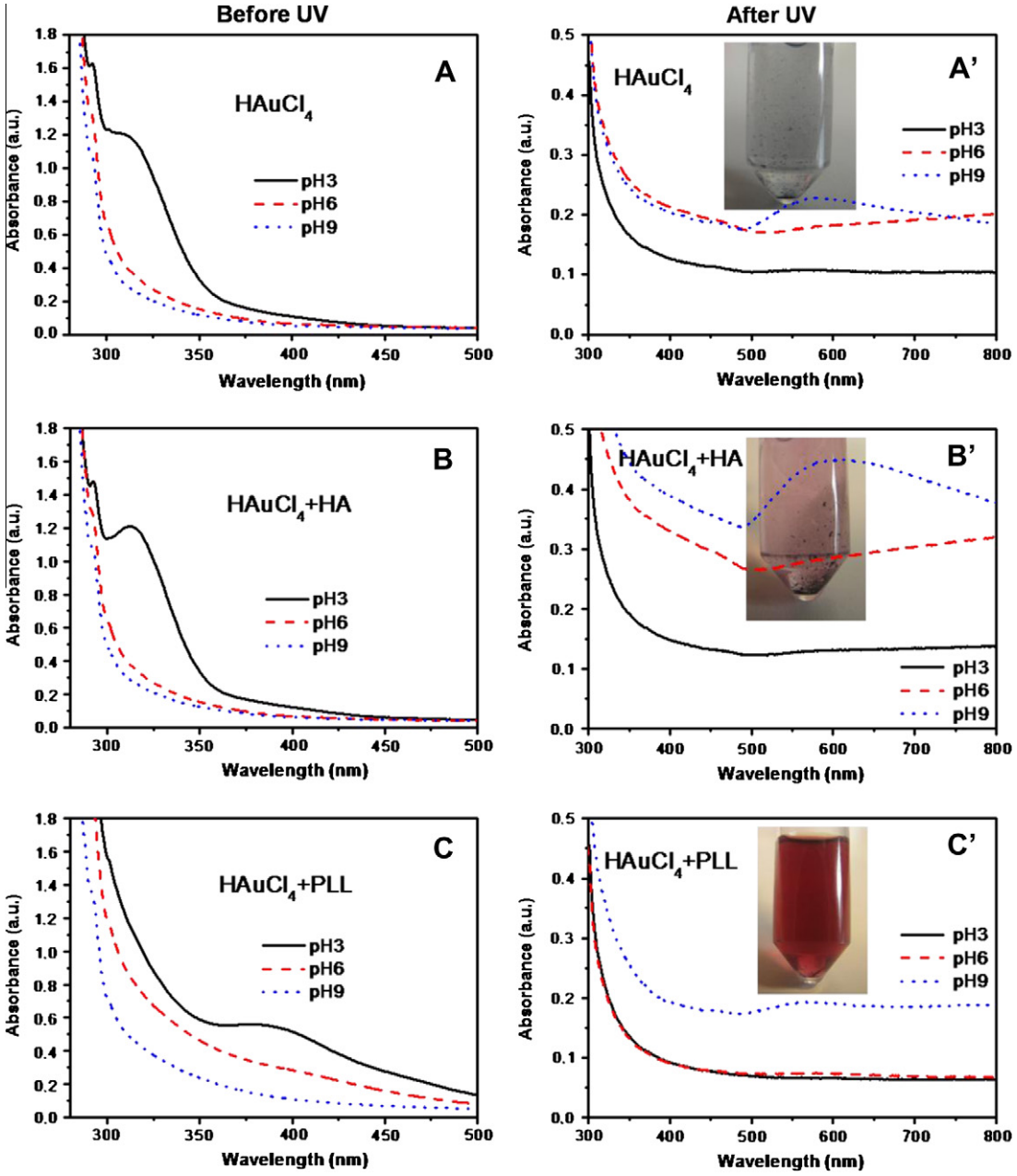

Fig. 5. UV–visible absorbance spectra of 1 mM $HAuCl_4$ solution (A, A′), 1 mM $HAuCl_4$ and 3 mg/mL hyaluronic acid solution (B, B′) and 1 mM $HAuCl_4$ and 1 mg/mL poly(L-lysine) solution (C, C′) at different pH before UV irradiation (left column) and after UV irradiation (right column). Insets are digital images of the same solutions obtained after UV irradiation at pH 9.

noticed a marked decrease in the COO^- peaks at 1604 cm^{-1} (also visible on the second peak at 1400 cm^{-1}) and a concomitant increase in COOH peak at 1735 cm^{-1}, especially at pH 3 (−40%) and to a lesser extent at pH 6 (−9.2%) (Fig. 6A and B and Table 2). This may be attributed to conversion of COO^- to COOH. Secondly, we observed a slight decrease of the peaks at 1047 cm^{-1} and 1078 cm^{-1}, indicating a change in the hydroxyl groups of HA [54]. Third, a significant increase was observed at ∼1656 cm^{-1}, corresponding to the amide band of PLL [40]. Again, the change was more pronounced at acidic pH (+18.7%) than as neutral pH (+2.5%). This change may originate from the interaction of PLL with gold ions. Of note, all the observed changes exhibited the same trends at all pH conditions, but they were more pronounced at pH 3 (Fig. 6A–C).

After UV-irradiation, the COO^- peaks as well as the hydroxyl peaks all further decreased (Fig. 6A′–C′ and Table 2). The amide I peak at 1656 cm^{-1} also decreased significantly. Again, the changes were more pronounced at pH 3 with a decrease of the order of 11–17% (Table 2). At pH 6 and 9, the changes were of the order of 6–9% at maximum. In parallel, there was a large increase of the COOH peak at 1735 cm^{-1}, which was also higher at pH 3.

All together, the FTIR data highlighted three major changes under UV-irradiation occurred: (1) conversion of COO^- to COOH, (2) decrease of H-bonded C—OH of alcohols and C—O—C in HA at 1047 cm^{-1} and 1078 cm^{-1} and (3) for the amide I of PLL, a decrease at 1656 cm^{-1}. The magnitude of the changes was in the order pH 9 < pH 6 < pH 3.

Thus, besides amine groups, HA molecules can be implicated in the photo-reduction process. Indeed, several studies have already shown that CH_2—OH groups, which are present in the backbone of HA, can facilitate gold ion reduction under photo irradiation

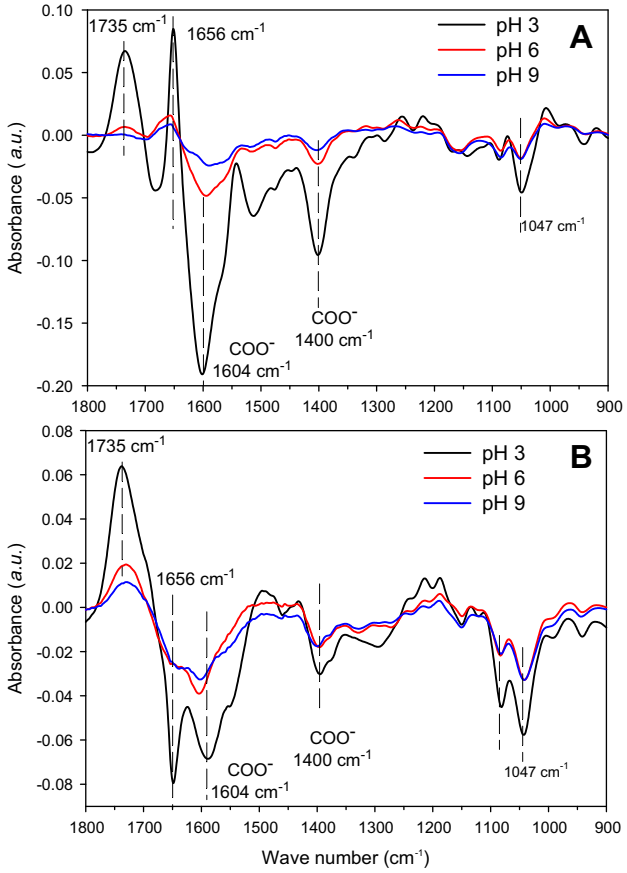

Fig. 6. FTIR characterization of gold salt loading and UV-irradiation in $(PLL9.5/HA2.9)_7$-PLL9.5 films. The colors represent the pH of the gold precursor solution: pH 3 (black line), pH 6 (red line) and pH 9 (blue line). (A) Differences between the FTIR spectra of the film measured after gold salt loading to that of the film measured before salt loading (i.e. "native" film); (B) differences between FTIR spectra of the film measured after UV irradiation to that measured before UV-irradiation (i.e., after gold salt loading). (For interpretation of the references to color in this figure legend, the reader is referred to the web version of this article.)

Table 2
Changes of the major peaks of the FTIR spectra measured as% of the initial value: Amide I (1656 cm^{-1}), COO^- (1604 cm^{-1}) and saccharide ring (1047 cm^{-1}) changes after contact with the chloroaurate solution, before or after UV irradiation, as compared to the initial values of these peaks for the $(PLL9.5/HA2.9)_7$-PLL9.5 films.

Peak (cm^{-1})	Before UV (%)			After UV (%)		
	pH 3	pH 6	pH 9	pH 3	pH 6	pH 9
1656	+18.7	+2.5	+1.2	−17.1	−5.7	−5.5
1604	−40.5	−9.2	−3.7	−12.7	−8.9	−7.3
1047	−9.1	−2.2	−2.2	−10.9	−6.8	−6.6

[26,55,56]. It has also been proven that hyaluronic acid can help the formation of silver NP under UV irradiation by oxidation of CH_2OH groups to CHO [57]. The carboxylic group itself might even play a role in the reduction of gold ions, as was recently suggested by Wang et al. [28] as it is a proton acceptor.

It is already acknowledged that the conformation and structure of an organic template are crucial parameters in the nucleation and/organization of inorganic nanoparticles [58,59]. Also, it is now well accepted that the synthesis of gold NPs involves a two-step process [56]. First, there is a nucleation step, in which part of the metal ions are reduced and act as nucleation centers. Second, the nucleation centers catalyze the reduction of the remaining metal ions present in the surrounding. The coalescence of atoms leads to the formation of metal clusters and these are effectively stabilized by ligands, surfactants or polymers.

Based on UV–visible spectrometry, FTIR data and TEM images, we propose the following mechanism for gold NP formation in $(PLL9.5/HA2.9)_7$-PLL9.5 films (Scheme 1). At pH 3, amine groups were mostly protonated in NH_3^+ groups and carboxyl groups were partially ionized (the pKa of PLL and HA are of ~9 and ~3, respectively), generating more free NH_3^+ groups and allowing maximal interactions with incoming $AuCl_4^-$ ions. The Au nucleation speed was slow but growth was steady, generating a lower number of NPs but of larger diameter (~8.7 nm).

At pH 6, both of the amine groups and the carboxyl groups were fully ionized, so there were fewer interactions with aurochlorate anions. The major form of gold ions was $Au^+Cl_2^-$ ions at this pH [49], so the nucleation process was faster than in case of pH 3. A larger number of gold NPs grew over the whole film thickness but their growth was limited to size of ~3 nm in diameter.

At pH 9, about half of the amine groups were protonated and COO^- groups of HA were fully ionized, allowing even fewer interactions with gold ions. At high pH, the $AuCl_2^-$ form was easily reduced and the number of nuclei was higher [50]. In fact it is proven that the nucleation of nanoparticles are favored in basic pH [6]. However, the NPs formed were rapidly stabilized by the amine groups and their growth was limited to ~2 nm. Indeed, this very small size was associated with the appearance of a very small SPR peak (Fig. 1C and C′) and with the absence of a clear diffraction pattern (Fig. 4C″).

In all cases, part of the CH_2—OH groups on HA chains served as reducing agents and turned to CHO and some COO^- groups converted to COOH after gold NP UV-reduction (which released H^+). The extent of these changes is related to the amount of gold NPs formed in the different conditions.

Thus, the large number of ammonium, carboxylic and hydroxyl groups as well as PLL diffusion within the film all contributed to the formation of homogenous NPs that were spatially-confined in the "bulk" of the film.

This simple and efficient "green" method to synthesize *in situ* in mild conditions a large number of gold NPs in exponentially-growing films of soft biopolymers appears very promising. The gold NPs spatially-confined in PEM films may advantageously be used to functionalize different types of materials or devices, as LbL films can be easily deposited on any solid substrates of any shape. The PEM-based nanocomposites may be employed as coating for imaging purpose or for biosensing. They may also find applications in the treatment of cancer as Au NPs efficiently convert the strongly absorbed light into localized heat, which can be exploited for the selective laser photothermal therapy of cancer [60].

3. Experimental section

3.1. Preparation of multilayer films

Poly(L-lysine) bromide (PLL, P2636, MW = 68 kDa) and gold chloride trihydrate ($HAuCl_4{\cdot}3H_2O$, 99.9% purity) were purchased from Sigma. Hyaluronic acid, (HA, MW = 1300 kDa) was a product of Fluka. 14 mm diameter glass slides (VWR Scientific, France) or silicon wafers (Siltronix SAS, Archamps, France) taken as substrates were cleaned by soaking in 2% (v/v) Hellmanex® II (Hellma GmbH, Müllheim, Germany) aqueous solution at 70 °C for 15 min, then rinsed thoroughly with water, and dried with a stream of nitrogen. The film was built by immersing the substrate alternately in PLL solution (1 mg/mL) at pH 9.5 and HA (3 mg/mL) at pH 2.9 with intermediate rinse in water of same pH and blowing dry. In this study, we built $(PLL9.5/HA2.9)_7$-PLL9.5 films (films made of 7.5

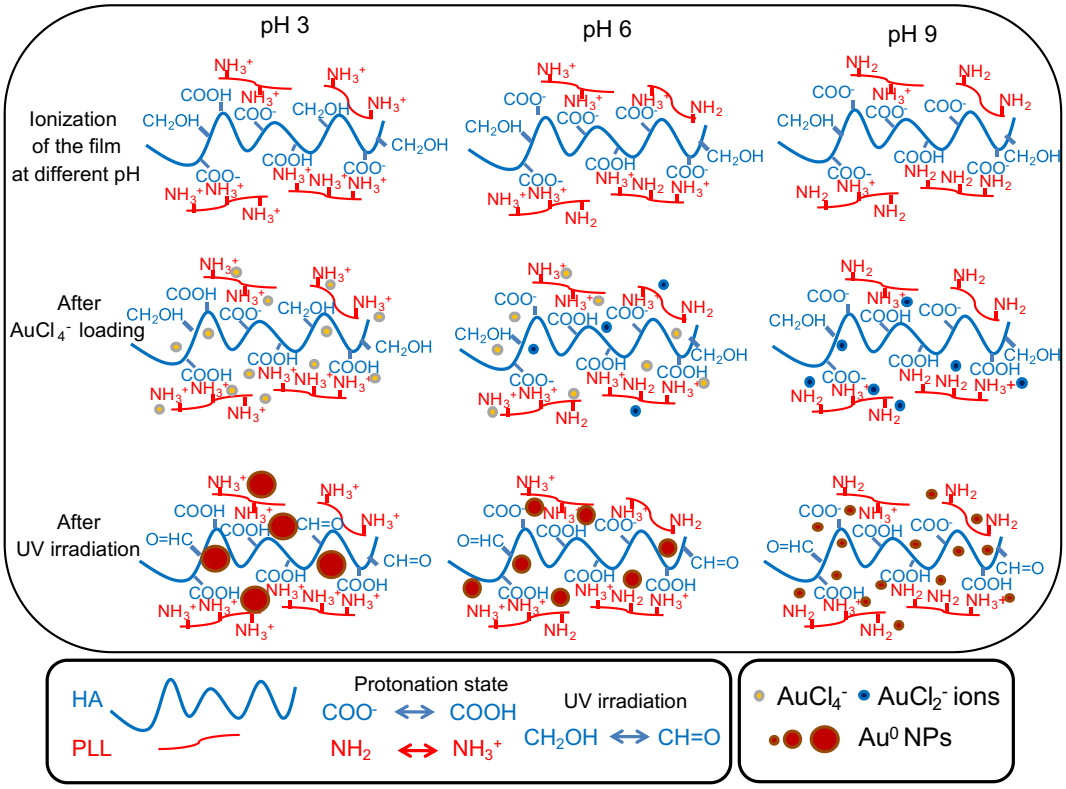

Scheme 1. Proposed mechanism for *in situ* formation of gold NP in (PLL9.5/HA2.9) PEM films at different pHs. The protonation degree of HA and PLL both depends on pH; the number of protonated COOH groups is higher at low pH and decreases when the pH is increased; Also, the number of protonated NH_3^+ groups decreases when the pH is increased. After $AuCl_4^-$ loading, the ions interact with NH_3^+ groups that were either free or paired with COO^- groups; thus, a fraction of COO^- groups becomes protonated in COOH; this fraction is higher at low pH of 3. $AuCl_4^-$ ions may also be reduced to $AuCl_2^-$ ions, especially at high pH of 9 and to some extent at pH 6. Both ions may associate with free H^+ ions of the films. After UV irradiation, gold NPs are formed in all conditions but the NPs are larger and less numerous at low pH (median size of ~8.6 nm). Their size decreases when the pH is increased to reach 3 nm at pH 6; In both conditions, UV–visible spectra showed a clear increase as a function of time and the diffraction pattern of Au was intense. At very high pH of 9, gold NPs have a small median diameter of 1.7 nm, but they have formed at a very high density in the film. However, due to their very small size, the UV–visible spectrum exhibits only a minor increase, the SPR peak is small and there is no diffraction signal. In all case, the CH_2OH groups of HA can be oxidized to CH=O during UV-irradiation.

layer pairs, ending by PLL) and $(PLL9.5/HA2.9)_8$ (films made of 8 layer pairs, ending by HA).

3.2. Gold NP in situ synthesis

For gold salt loading, the PLL-ending or HA-ending films were immersed into 10 mM gold chloride salt solution for 15 min, followed by three water rinses, before being air dried in an incubator at 37 °C for 30 min. As the pH of the 10 mM gold chloride solution is ~2, NaOH was added drop wise until the desired pH was achieved. The gold-salt-loaded samples were irradiated with an ultra violet lamp (365 nm, VL-215.LC, France, Power = 30 W) at a distance of ~1 cm for 35 h, as described by others [12].

3.3. Fourier transform infrared spectroscopy

Film structure was investigated by Fourier transform infrared (FTIR) spectroscopy in transmission mode using a Vertex 70 spectrophotometer (Bruker Optics GmbH, Ettlingen, Germany) equipped with a mid-infrared (MIR) detector. All the films were deposited on silicon wafers for these experiments. The spectrum from the bare Si was always taken as reference. A single-channel spectrum from 256 interferograms was recorded between 400 and 4000 cm^{-1} with a 2 cm^{-1} resolution, using Blackman-Harris three-term apodization and the standard Bruker OPUS/IR software v6.5 (Bruker Optics GmbH). The different peaks characteristic of the polyelectrolytes and of the pH-amplified (PLL/HA) films have identified in our previous work [40]. Basically, there are three absorption regions in the FTIR spectra. The band from 3500 to 3000 cm^{-1} is mainly associated with hydrogen bonded N—H and O—H groups. The region from 1750 to 1350 cm^{-1} contains COOH (1735 cm^{-1}), amide I (1656 cm^{-1}, random), amide II (1560 cm^{-1}) and COO^- (1605 and 1400 cm^{-1}). The characteristic peaks of saccharide rings on HA are visible in the 960–1200 cm^{-1} region, with the most intensive peaks at 1045 and 1080 cm^{-1}.

3.4. UV–visible spectrometry

Films were built on 14 mm-diameter glass slides and their UV–visible spectra were taken using a spectrofluorimeter (Infinite M1000, Tecan, Australia) at predetermined time interval to follow the reduction process. The wavelength ranges from 230 nm to 800 nm with 1 nm step size. The bandwidth was of 2.5 nm over the range 230–300 nm and of 5 nm over the range 301–800 nm.

3.5. Inductively coupled plasma mass spectrometry (ICP-MS)

The amount of Au nanoparticle loaded in the films were determined by a Inductively Coupled Plasma Mass Spectrometry (ICP-MS, X-series, Thermo Corporation Inc, USA). Films embedded with Au nanoparticle of a certain surface (around 5 × 4 mm^2) were put into 1 mL freshly prepared aqua regia (HNO_3: HCl *v*:*v* = 1:3) for 10 min to turn Au^0 to Au ions. Finally, the solutions were diluted

to 200 mL and the Au ion concentrations were quantified by ICP-MS.

3.6. Scanning electron microscopy

For SEM observations, the PLL-ending (7.5 layer pairs) or HA-ending (8 layer pairs) films were prepared on silicon wafer following the procedure described above. The surface morphology and the cross-section of the NPs synthesized in the films were visualized by using a field emission gun (FEG) SEM (Quanta FEG 250, FEI, Czech Republic). The low voltage high contrast (vCD) detector mode was used to enhance the element contrast and better identify the gold NPs.

3.7. Atomic force microscopy

The surface morphology of films with or without gold NPs was imaged in tapping mode using a Veeco Di 3100 AFM (Veeco, France) with OMCT-240 tapping mode cantilevers (Olympus, France). The final images were treated with Gwyddion software version 2.22.

3.8. Transmission electron microscopy

The cross-section morphology of nanocomposite films was monitored by transmission electron microscopy (TEM) and high-resolution TEM (HR-TEM) using a JEM-2100 LaB6 (JEOL, Japan) operating at 200 kV with a 0.19 nm point-to-point resolution. Two pieces of film-coated silicon were embedded face-to-face in epoxy (M-bond 610) for 2 h at 150 °C such as to form a silicon-film-resin-film-silicon sandwich ($\sim 1.5 \times 2 \times 2.5\ mm^3$). This sandwich was further cut into 2–3 pieces before being polished by the tripod polishing method [61]. To this end, the specimen was glued onto the glass stub of the tripod polisher (model 590 TEM, South Bay Technology, San Clemente, USA). Samples were polished on both sides using a series of plastic diamond lapping films (Escil, Lyon, France), with grains of decreasing sizes (30 μm, 15 μm, 6 μm, 1 μm, 0.5 μm respectively). The first side of the sandwich was polished to achieve a 300–500 μm in thickness. Then, it was reverted to continue with the polishing of the second side, the sample being tilted at an angle ~0.6°. An optical inverted microscope was used to check frequently the residual specimen thickness so as to obtain a thickness <10–15 μm. Finally, the sample was removed from the glass stub and glued onto a TEM copper grid containing a central hole. Low-angle ion beam milling (Gatan, Colorado, USA) was used for the final precision polishing of the samples. The final thickness around the perforated area is <100 nm. Energy dispersive X-ray (EDAX) spectra were also collected perpendicular to the sample surface.

3.9. Image analysis

Particle size was measured for each sample using Image J software v1.38x (NIH Bethesda, USA, http://rsbweb.nih.gov/ij/index.html) The reported particle sizes are the number average from at least 240 particles. The particle size distribution was also generated by Sigma Plot software (Systat, USA).

4. Conclusions

We prepared a nanocomposite film using exponentially growing polyelectrolyte multilayer films as a nanoreservoir to synthesize *in situ* gold NPs in a spatially-confined 2D environment. The process was easily achieved by loading gold ions from an aqueous solution, then irradiating the dry film under UV light. Gold NPs of ~2 nm to ~9 nm in diameter were successfully formed at a high yield. They were distributed homogeneously throughout the whole film thickness (~2.5 μm). Besides the ammonium groups of PLL, which interacted with chloroaurate ions and stabilized the formed NPs, carboxylic and hydroxyl groups of HA played a key role in the formation of gold NPs. Thus, the efficient nucleation and growth of gold NPs appeared to be dependent on the presence of specific functional groups in the film and on the mobility and even distribution of PLL in the film as well. Other exponentially-growing polypeptide and polysaccharide PEM films that present a charge imbalance between the polyelectrolytes may be further used to synthesize a large variety of gold NPs. The gold NPs/PEM nanocomposites containing a very high amount of gold NPs may find applications as biosensors, drug reservoirs or for imaging of opaque materials.

Acknowledgments

C.P. is a Junior Member of the "Institut Universitaire de France" whose support is gratefully acknowledged. C.P. is grateful to the European Research Council for financial support (ERC Starting Grant 259370). L.S. thanks the French government ("Eiffel Doctorat" program) and the French Embassy in China for financial support. J.J. thanks the financial support from the NSFC-50830106 and China National Funds for Distinguished Young Scientists (51025312). We would like to thank Didier Delabouglise, Michel Langlet and Roland Madar for fruitful discussions and Simon LeDemnat for technical assistance.

Appendix A. Supplementary material

Supplementary data associated with this article can be found, in the online version, at http://dx.doi.org/10.1016/j.jcis.2012.06.079.

References

[1] H.W. Liao, C.L. Nehl, J.H. Hafner, Nanomedicine 1 (2006) 201–208.
[2] B. Sepulveda, P.C. Angelome, L.M. Lechuga, L.M. Liz-Marzan, Nano Today 4 (2009) 244–251.
[3] J.N. Anker, W.P. Hall, O. Lyandres, N.C. Shah, J. Zhao, R.P. Van Duyne, Nat. Mater. 7 (2008) 442–453.
[4] C.J. Murphy, A.M. Gole, S.E. Hunyadi, J.W. Stone, P.N. Sisco, A. Alkilany, B.E. Kinard, P. Hankins, Chem. Commun. (2008) 544–557.
[5] X.H. Huang, P.K. Jain, I.H. El-Sayed, M.A. El-Sayed, Nanomedicine 2 (2007) 681–693.
[6] I. Pastoriza-Santos, R.A. Alvarez-Puebla, L.M. Liz-Marzan, Eur. J. Inorg. Chem. (2010) 4288–4297.
[7] C.L. Chen, N.L. Rosi, Angew. Chem., Int. Ed. 49 (2010) 1924–1942.
[8] A.A. Galyean, R.W. Day, J. Malinowski, K.W. Kittredge, M.C. Leopold, J. Colloid Interface Sci. 331 (2009) 532–542.
[9] W. Schrof, S. Rozouvan, E. Van Keuren, D. Horn, J. Schmitt, G. Decher, Adv. Mater. 10 (1998) 338–341.
[10] W.F. Dong, G.B. Sukhorukov, H. Mohwald, Phys. Chem. Chem. Phys. 5 (2003) 3003–3012.
[11] D. Lee, M.F. Rubner, R.E. Cohen, Nano Lett. 6 (2006) 2305–2312.
[12] K.K. Chia, R.E. Cohen, M.F. Rubner, Chem. Mater. 20 (2008) 6756–6763.
[13] K. Esumi, A. Suzuki, N. Aihara, K. Usui, K. Torigoe, Langmuir 14 (1998) 3157–3159.
[14] E.E. Connor, J. Mwamuka, A. Gole, C.J. Murphy, M.D. Wyatt, Small 1 (2005) 325–327.
[15] D. Toroz, S. Corni, Nano Lett. 11 (2011) 1313–1318.
[16] Y.N. Tan, J.Y. Lee, D.I.C. Wang, J. Am. Chem. Soc. 132 (2010) 5677–5686.
[17] X.Q. Cui, C.M. Li, H.F. Bao, X.T. Zheng, Z.S. Lu, J. Colloid Interface Sci. 327 (2008) 459–465.
[18] M.J. Richardson, J.H. Johnston, T. Borrmann, Eur. J. Inorg. Chem. (2006) 2618–2623.
[19] S. Joly, R. Kane, L. Radzilowski, T. Wang, A. Wu, R.E. Cohen, E.L. Thomas, Langmuir 16 (2000) 1354–1359.
[20] R. Sardar, N.S. Bjorge, J.S. Shumaker-Parry, Macromolecules 41 (2008) 4347–4352.
[21] M. Hu, J.Y. Chen, Z.Y. Li, L. Au, G.V. Hartland, X.D. Li, M. Marquez, Y.N. Xia, Chem. Soc. Rev. 35 (2006) 1084–1094.
[22] E. Boisselier, D. Astruc, Chem. Soc. Rev. 38 (2009) 1759–1782.
[23] Y. Mei, G. Sharma, Y. Lu, M. Ballauff, M. Drechsler, T. Irrgang, R. Kempe, Langmuir 21 (2005) 12229–12234.

[24] J.H. Cho, F. Caruso, Chem. Mater. 17 (2005) 4547–4553.
[25] J.D.S. Newman, G.J. Blanchard, Langmuir 22 (2006) 5882–5887.
[26] K. Mallick, M.J. Witcomb, M.S. Scurrell, Appl. Phys. A – Mater. Sci. Process. 80 (2005) 395–398.
[27] T. Kar, S. Dutta, P.K. Das, Soft Matter 6 (2010) 4777–4787.
[28] Y.N. Tan, J.Y. Lee, D.I.C. Wang, J. Phys. Chem. C 113 (2009) 10887–10895.
[29] E. Kharlampieva, J.M. Slocik, T. Tsukruk, R.R. Naik, V.V. Tsukruk, Chem. Mater. 20 (2008) 5822–5831.
[30] G. Decher, Science 277 (1997) 1232–1237.
[31] D. Yoo, S.S. Shiratori, M.F. Rubner, Macromolecules 31 (1998) 4309–4318.
[32] W.Y. Yuan, J.H. Fu, K. Su, J. Ji, Colloids Surf. B 76 (2010) 549–555.
[33] A. Agarwal, T.L. Weis, M.J. Schurr, N.G. Faith, C.J. Czuprynski, J.F. McAnulty, C.J. Murphy, N.L. Abbott, Biomaterials 31 (2010) 680–690.
[34] T.C. Wang, R.E. Cohen, M.F. Rubner, Adv. Mater. 14 (2002) 1534–1537.
[35] F. Caruso, K. Niikura, D.N. Furlong, Y. Okahata, Langmuir 13 (1997) 3422–3426.
[36] J.A. Jaber, J.B. Schlenoff, Langmuir 23 (2007) 896–901.
[37] C. Picart, P. Lavalle, P. Hubert, F.J.G. Cuisinier, G. Decher, P. Schaaf, J.-C. Voegel, Langmuir 17 (2001) 7414–7424.
[38] C. Picart, J. Mutterer, L. Richert, Y. Luo, G.D. Prestwich, P. Schaaf, J.-C. Voegel, P. Lavalle, Proc. Natl. Acad. Sci. USA 99 (2002) 12531–12535.
[39] T. Crouzier, C. Picart, Biomacromolecules 10 (2009) 433–442.
[40] L. Shen, P. Chaudouet, J. Ji, C. Picart, Biomacromolecules 12 (2011) 1322–1331.
[41] X. Wang, J. Ji, Langmuir 25 (2009) 11664–11671.
[42] A.J. Haes, S.L. Zou, G.C. Schatz, R.P. Van Duyne, J. Phys. Chem. B 108 (2004) 6961–6968.
[43] S. Link, M.A. El-Sayed, Int. Rev. Phys. Chem. 19 (2000) 409–453.
[44] S. Eustis, M.A. El-Sayed, J. Phys. Chem. B 110 (2006) 14014–14019.
[45] S. Eustis, M.A. El-Sayed, Chem. Soc. Rev. 35 (2006) 209–217.
[46] G. Parks, Chem. Rev. 65 (1965) 177–198.
[47] J. Hiller, J.D. Mendelsohn, M.F. Rubner, Nat. Mater. 1 (2002) 59–63.
[48] A.K. Gangopadhayay, C. Chakravorty, J. Chem. Phys. 35 (1961) 4.
[49] G.H. Kelsall, N.J. Welham, M.A. Diaz, J. Electroanal. Chem. 361 (1993) 13–24.
[50] K. Kurihara, J. Kizling, P. Stenius, J.H. Fendler, J. Am. Chem. Soc. 105 (1983) 2574–2579.
[51] S. Eustis, H.Y. Hsu, M.A. El-Sayed, J. Phys. Chem. B 109 (2005) 4811–4815.
[52] F. Kim, S. Connor, H. Song, T. Kuykendall, P.D. Yang, Angew. Chem., Int. Ed. 43 (2004) 3673–3677.
[53] P.Y. Silvert, K. Tekaiaelhsissen, Solid State Ionics 82 (1995) 53–60.
[54] K. Haxaire, Y. Marechal, M. Milas, M. Rinaudo, Biopolymers 72 (2003) 10–20.
[55] S. Eustis, M.A. El-Sayed, J. Phys. Chem. B 109 (2005) 16350–16356.
[56] K. Mallick, M.J. Witcomb, M.S. Scurrell, Appl. Phys. A – Mater. Sci. Process. 80 (2005) 797–801.
[57] X.Q. Cui, C.M. Li, H.F. Bao, X.T. Zheng, J.F. Zang, C.P. Ooi, J. Guo, J. Phys. Chem. C 112 (2008) 10730–10734.
[58] H. Lee, S.H. Choi, T.G. Park, Macromolecules 39 (2006) 23–25.
[59] C.L. Chen, P. Zhang, N.L. Rosi, J. Am. Chem. Soc. 130 (2008) 13555–13557.
[60] P.K. Jain, I.H. El-Sayed, M.A. El-Sayed, Nano Today 2 (2007) 18–29.
[61] J. Ayache, P.H. Albarede, Ultramicroscopy 60 (1995) 195–206.